



**HAL**  
open science

## Inherited human Apollo deficiency causes severe bone marrow failure and developmental defects

Laëtitia Kermasson, Dmitri Churikov, Aya Awad, Riham Smoom, Elodie Lainey, Fabien Touzot, Séverine Audebert-Bellanger, Sophie Haro, Laureline Roger, Emilia Costa, et al.

► **To cite this version:**

Laëtitia Kermasson, Dmitri Churikov, Aya Awad, Riham Smoom, Elodie Lainey, et al.. Inherited human Apollo deficiency causes severe bone marrow failure and developmental defects. *Blood*, 2022, 10.1182/blood.2021010791/1858808/blood.2021010791.pdf . hal-03622423v1

**HAL Id: hal-03622423**

**<https://hal.sorbonne-universite.fr/hal-03622423v1>**

Submitted on 11 Jan 2022 (v1), last revised 15 Mar 2023 (v2)

**HAL** is a multi-disciplinary open access archive for the deposit and dissemination of scientific research documents, whether they are published or not. The documents may come from teaching and research institutions in France or abroad, or from public or private research centers.

L'archive ouverte pluridisciplinaire **HAL**, est destinée au dépôt et à la diffusion de documents scientifiques de niveau recherche, publiés ou non, émanant des établissements d'enseignement et de recherche français ou étrangers, des laboratoires publics ou privés.



American Society of Hematology  
2021 L Street NW, Suite 900,  
Washington, DC 20036  
Phone: 202-776-0544 | Fax 202-776-0545  
editorial@hematology.org

## Inherited human Apollo deficiency causes severe bone marrow failure and developmental defects

Tracking no: BLD-2021-010791R2

Laëtitia Kermasson (Institut IMAGINE UMR1163, France) Dmitri Churikov (Marseille Cancer Research Center, France) Aya Awad (The Silberman Institute of Life Science, Israel) Riham Smoom (The Silberman Institute of Life Science, Israel) Elodie Lainey (AP-HP - Hopital Robert Debré, France) Fabien Touzot (CHU Sainte-Justine, Canada) Séverine Audebert-Bellanger (Department of medical genetics,, France) Sophie Haro (Department of paediatrics and medical genetics,, France) Laureline Roger (Muséum National d'Histoire Naturelle, France) Emilia Costa (Centro Hospitalar e Universitário do Porto, Portugal) Maload Mouf (Zenon Skelter Institute, Norway) Adriana Bottero (Servicio de Gastroenterología. Hospital de Pediatría "Prof. Dr. Juan P. Garrahan",, Argentina) Matias Oleastro (Garrahan Hospital, Argentina) Chrystelle Abdo (Hopital Necker, Université de Paris, France) Jean-Pierre de Villartay (AP-HP, Hopital Necker Enfants Malades, Service d'Immunologie et d'Hématologie Pédiatrique, France) Vincent Géli (U1068 Inserm, UMR7258 CNRS, Aix-Marseille University, Institut Paoli-Calmettes, France) Yehuda Tzfati (The Hebrew University of Jerusalem, Israel) ISABELLE CALLEBAUT (Sorbonne University, CNRS UMR7590, Museum National d'Histoire Naturelle, France) Silvia Danielian ("Juan Pedro Garrahan" National Hospital of Pediatrics, Argentina) Gabriela Soares (Centro de Genética Médica Jacinto de Magalhães, Portugal) Caroline Kannengiesser (APHP, Hopital Xavier Bichat, Service de Génétique, France) Patrick Revy (Imagine Institute for Genetic Diseases, France)

### Abstract:

Inherited bone marrow failure syndromes (IBMFS) represent a group of disorders typified by impaired production of one or several blood cell types. The telomere biology disorders dyskeratosis congenita (DC) and its severe variant Høyeraal-Hreidarsson (HH) syndrome are rare IBMFS characterized by bone marrow failure, developmental defects, and various premature aging complications associated with critically short telomeres. Here we identified biallelic variants in the gene encoding the 5'-to-3' DNA exonuclease Apollo/SNM1B in three unrelated patients presenting with a DC/HH phenotype consisting of early onset hypocellular bone marrow failure, B and NK lymphopenia, developmental anomalies, microcephaly and/or intrauterine growth retardation. All three patients carry a homozygous or compound heterozygous (in combination with a null-allele) missense variant affecting the same residue L142 (L142F or L142S) located in the catalytic domain of Apollo. Apollo-deficient cells from patients exhibited spontaneous chromosome instability and impaired DNA repair that was complemented by CRISPR/Cas9-mediated gene correction. Furthermore, patients' cells showed signs of telomere fragility that were however not associated with global reduction of telomere length. Unlike patients' cells, human Apollo KO HT1080-cell lines showed strong telomere dysfunction accompanied by excessive telomere shortening, suggesting that the L142S and L142F Apollo variants are hypomorphic. Collectively, these findings define human Apollo as a genome caretaker and identify biallelic Apollo variants as a genetic cause of a hitherto unrecognized severe IBMFS combining clinical hallmarks of DC/HH with normal telomere length.

**Conflict of interest:** No COI declared

**COI notes:**

**Preprint server:** No;

**Author contributions and disclosures:** Authorship contributions. L.K. carried out most of the experimental work. D.C. performed TeSLA analysis. A.A. and R.S. performed in-gel hybridization experiments. L.R. participated to the initial characterization of the shortest telomeres. P.R., C.K., S.D. and G.S. performed genetic analysis and identified Apollo mutations. S. A-B., S.H., E.C., M.O., F.T., S.D., and G.S. identified the affected patients and assisted with related clinical and laboratory studies. E.L. performed Flow-FISH. M.M. provided intellectual input. C.A. performed TCR repertoire analysis. I.C. performed structural analysis. P.R. conceived the project and wrote the manuscript with editing contributions from J-P.V., F.T., I.C., V.G., and Y.T.

**Non-author contributions and disclosures:** No;

**Agreement to Share Publication-Related Data and Data Sharing Statement:** The deposit of the Results from DNA sequencing of Apollo is ongoing.

Clinical trial registration information (if any):

1 **Inherited human Apollo deficiency causes severe bone marrow failure**  
2 **and developmental defects**  
3  
4

5 Laëtitia Kermasson<sup>1</sup>, Dmitri Churikov<sup>2</sup>, Aya Awad<sup>3</sup>, Riham Smoom<sup>3</sup>, Elodie Lainey<sup>4</sup>, Fabien Touzot<sup>5</sup>,  
6 Séverine Audebert-Bellanger<sup>6</sup>, Sophie Haro<sup>6</sup>, Lauréline Roger<sup>7</sup>, Emilia Costa<sup>8</sup>, Maload Mouf<sup>9</sup>, Adriana  
7 Bottero<sup>10</sup>, Matias Oleastro<sup>11</sup>, Chrystelle Abdo<sup>12</sup>, Jean-Pierre de Villartay<sup>1</sup>, Vincent Géli<sup>2</sup>, Yehuda  
8 Tzfati<sup>3</sup>, Isabelle Callebaut<sup>13</sup>, Silvia Danielian<sup>14</sup>, Gabriela Soares<sup>15</sup>, Caroline Kannengiesser<sup>16</sup>, Patrick  
9 Revy<sup>1,\*</sup>.

10  
11 <sup>1</sup> Université de Paris, Imagine Institute, Laboratory of Genome Dynamics in the Immune System,  
12 Laboratoire labellisé Ligue, INSERM UMR 1163, F-75015, Paris, France

13 <sup>2</sup> Marseille Cancer Research Center (CRCM), U1068 Inserm, UMR7258 CNRS, Institut Paoli-  
14 Calmettes, Aix Marseille University, Marseille, France. Equipe labélisée Ligue National Contre le  
15 Cancer.

16 <sup>3</sup> Department of Genetics, The Silberman Institute of Life Science, The Hebrew University of  
17 Jerusalem, Safra Campus—Givat Ram, Jerusalem 91904, Israel

18 <sup>4</sup> Hematology Laboratory, Robert DEBRE Hospital-APHP and INSERM UMR 1131-Hematology  
19 University Institute-Denis Diderot School of Medicine, Paris, France

20 <sup>5</sup> CHU Sainte Justine Research Center, Montréal, Quebec, Canada; Université de Montréal, Montréal,  
21 Quebec, Canada; Department of Immunology-Rheumatology, Department of Pediatrics, CHU Sainte  
22 Justine, Montréal, Quebec, Canada

23 <sup>6</sup> Department of paediatrics and medical genetics, CHU de Brest, 2, avenue Foch, 29609 Brest cedex,  
24 France

25 <sup>7</sup> Structure and Instability of Genomes laboratory, “Muséum National d’Histoire Naturelle” (MNHN),  
26 Inserm U1154, CNRS UMR 7196, Paris, France

27 <sup>8</sup> Serviço de Pediatria, Centro Hospitalar e Universitário do Porto, EPE, Porto, Portugal

28 <sup>9</sup> Zenon Skelter Institute, Meddle Laboratory, 68 HAL, 310391-JM, Green Hills, Eggum, Norway



29 <sup>10</sup> Servicio de Gastroenterología. Hospital de Pediatría "Prof. Dr. Juan P. Garrahan", Buenos Aires,  
30 Argentina

31 <sup>11</sup> Rheumatology and Immunology Service, Hospital Nacional de Pediatría JP Garrahan, Buenos  
32 Aires, Argentina

33 <sup>12</sup> Onco-Hematology, Assistance Publique-Hôpitaux de Paris, Université de Paris and Institut Necker  
34 Enfants Malades, Paris, France

35 <sup>13</sup> Sorbonne Université, Muséum National d'Histoire Naturelle, UMR CNRS 7590, Institut de  
36 Minéralogie, de Physique des Matériaux et de Cosmochimie, IMPMC, 75005 Paris, France

37 <sup>14</sup> Department of Immunology, "Juan P. Garrahan" National Hospital of Pediatrics, Buenos Aires,  
38 Argentina

39 <sup>15</sup> Centro de Genética Médica Jacinto de Magalhães, Centro Hospitalar e Universitário do Porto, EPE,  
40 Porto, Portugal

41 <sup>16</sup> Assistance Publique des Hôpitaux de Paris, Hôpital Bichat, Service de Génétique, Université Paris  
42 Diderot, Paris, France

43 \*Corresponding author: Patrick Revy; patrick.revy@cns.fr; Tel. (33) 1 42 75 42 92

44

45

46 **Keywords:** Telomere, Apollo, Inherited bone marrow failure syndrome, DNA repair, dyskeratosis  
47 congenita, Høyeraal-Hreidarsson syndrome

48

49 **Running title:** Human Apollo deficiency causes IBMFS

50

#### 51 **KEY POINTS**

- 52 • Biallelic Apollo variants cause a bone marrow failure syndrome with clinical hallmarks of  
53 dyskeratosis congenita but normal telomere length
- 54 • Apollo is a genome caretaker critical for the proper development of the immuno-hematological  
55 system in humans.

56

57

58

59 **ABSTRACT**

60 Inherited bone marrow failure syndromes (IBMFS) represent a group of disorders typified by impaired  
61 production of one or several blood cell types. The telomere biology disorders dyskeratosis congenita  
62 (DC) and its severe variant Høyeraal-Hreidarsson (HH) syndrome are rare IBMFS characterized by  
63 bone marrow failure, developmental defects, and various premature aging complications associated  
64 with critically short telomeres. Here we identified biallelic variants in the gene encoding the 5'-to-3'  
65 DNA exonuclease Apollo/SNM1B in three unrelated patients presenting with a DC/HH phenotype  
66 consisting of early onset hypocellular bone marrow failure, B and NK lymphopenia, developmental  
67 anomalies, microcephaly and/or intrauterine growth retardation. All three patients carry a homozygous  
68 or compound heterozygous (in combination with a null-allele) missense variant affecting the same  
69 residue L142 (L142F or L142S) located in the catalytic domain of Apollo. Apollo-deficient cells from  
70 patients exhibited spontaneous chromosome instability and impaired DNA repair that was  
71 complemented by CRISPR/Cas9-mediated gene correction. Furthermore, patients' cells showed signs  
72 of telomere fragility that were however not associated with global reduction of telomere length. Unlike  
73 patients' cells, human Apollo KO HT1080-cell lines showed strong telomere dysfunction accompanied  
74 by excessive telomere shortening, suggesting that the L142S and L142F Apollo variants are  
75 hypomorphic. Collectively, these findings define human Apollo as a genome caretaker and identify  
76 biallelic *Apollo* variants as a genetic cause of a hitherto unrecognized severe IBMFS combining clinical  
77 hallmarks of DC/HH with normal telomere length.

78

79

80

81

82

83

84

85

86

87

## 88 INTRODUCTION

89 Inherited bone marrow failure syndromes (IBMFS) represent heterogeneous Mendelian  
90 diseases having in common an impaired production of one or several blood cell lineages<sup>1</sup>. Growth  
91 delay, mucocutaneous abnormalities, developmental defects and cancer predisposition are other  
92 clinical outcomes that can manifest in IBMFS<sup>1</sup>. Dyskeratosis congenita (DC) and its severe variant  
93 Høyeraal-Hreidarsson (HH) syndrome are rare IBMFS. DC is mainly characterized by progressive  
94 bone marrow failure, premature aging manifestations and increased cancer predisposition, while HH  
95 can associate with early-onset bone marrow failure, intrauterine growth retardation (IUGR),  
96 microcephaly and/or cerebellar hypoplasia and immunodeficiency<sup>2,3</sup>. Since DC and HH are caused by  
97 genetic defects impacting the integrity and/or the length of telomeres, they belong to a heterogeneous  
98 group of conditions termed telomere biology disorders (TBDs)<sup>2-5</sup>. Telomeres are constituted by double-  
99 stranded TTAGGG repeats terminated by a 3' single-stranded sequence called G-overhang.  
100 Telomeres are decorated by a complex named shelterin<sup>6</sup> composed of six proteins (TRF1, TRF2,  
101 TIN2, RAP1, TPP1, POT1) among which TRF1 and TRF2 bind directly to the duplex telomeric DNA  
102 while POT1 binds to the single-strand G-overhang<sup>6</sup>. Shelterin is essential to protect chromosome  
103 from degradation and/or fusion and to maintain telomere length<sup>7</sup>. To date, variants in 11 factors  
104 (TERT, TERC, Dyskerin, NOP10, NHP2, TCAB1, TIN2, TPP1, CTC1, RTEL1, and PARN) that  
105 participate in telomere biology have been found to cause DC and HH<sup>2,3,8</sup>. In DC and HH, the severity  
106 and onset of symptoms are generally correlated to the degree of telomere length reduction<sup>9,10</sup>. Thus,  
107 telomere length determination is an effective approach to diagnose DC/HH in patients with IBMFS  
108<sup>2,10,11</sup>.

109 Apollo (SNM1B), encoded by the *DNA cross-link repair 1B (DCLRE1B/Apollo*; NC\_000001.11)  
110 gene, is a 5'-to-3' DNA exonuclease that functions within the Fanconi anemia (FA) pathway and is  
111 involved in the repair of both mitomycin C (MMC)-induced DNA interstrand crosslinks (ICL) and DNA  
112 double-strand breaks (DSB)<sup>12</sup> as well as the stabilization of stalled replication forks and S-phase  
113 checkpoint activation<sup>13-17</sup>. Moreover, the identification of single nucleotide polymorphisms in the  
114 *DCLRE1B/Apollo* locus associated with breast cancers and cutaneous melanoma supported a  
115 protective role of Apollo in genome integrity<sup>18,19</sup>.

116 Apollo also participates in telomere protection via an interaction between its TRFH Binding  
117 Motif (TBM) and the Telomeric Repeat Factors Homology (TRFH) domain of TRF2<sup>20-23</sup>. Apollo KO  
118 mouse embryonic fibroblasts (MEFs) exhibited impaired production of G-overhangs and frequent  
119 telomere fusions at the newly-replicated leading-end telomeres. This observation suggested that the  
120 nuclease activity of Apollo is involved in the generation of G-overhang that avoids fusion of leading  
121 telomeres<sup>24-26</sup>. In human cells, the role of Apollo at telomeres is less clear since its depletion induces  
122 telomere fragility causing multiple telomeric signals (MTS), that is however not associated with  
123 impaired G-overhang, increased telomere fusion or telomere shortening<sup>20,21</sup>. Nonetheless, it has been  
124 demonstrated that human Apollo together with TRF2 and the topoisomerase TopoIIa function in DNA  
125 replication of telomeric sequences by alleviating topological stress<sup>23</sup>.

126 We previously described a HH patient expressing an aberrantly spliced *Apollo* transcript  
127 leading to the production of a truncated Apollo that exerted a dominant negative effect on the stability  
128 of telomeres without affecting their global length<sup>27</sup>. Nonetheless, because we failed to identify the  
129 origin of the splice anomaly, we were unable to demonstrate a causal link between the truncated form  
130 of Apollo and the patient's clinical features<sup>27</sup>. Thus, although Apollo appears to be important for  
131 telomere stability and genome integrity, its relative contribution to telomere maintenance and DNA  
132 repair remains elusive, especially in humans.

133 Here, we identified biallelic *Apollo/DCLRE1B* variants in children exhibiting clinical features  
134 akin to DC/HH that are, however, not associated with decreased telomere length. Our study defines  
135 human Apollo as a genome caretaker.

136  
137  
138  
139  
140  
141  
142  
143  
144

145 **MATERIALS and METHODS**

146 **Patients** Informed consent was obtained from the families in accordance with the Declaration of  
147 Helsinki. The institutional INSERM and Assistance Publique–Hôpitaux de Paris review boards  
148 approved this study.

149 **Cells.** Cells used in this study are described in supplemental Materials and Methods.

150 **Telomere length measurement by fluorescence *in-situ* hybridization and flow cytometry and**  
151 **Telomere restriction fragment analysis (TRF).** The procedures for telomere length measurements  
152 are detailed in supplemental Materials and Methods.

153 **Whole exome sequencing and gene targeted sequencing.** Sequencing approaches are detailed in  
154 supplemental Materials and Methods.

155 **Telomere Shortest Length Assay (TeSLA).** TeSLA method, performed as described by Lai et al. <sup>28</sup>,  
156 is described in supplemental Materials and Methods.

157 **Telomeric FISH.** Telomeric FISH procedure is described in supplemental Materials and Methods.

158 **Detection of telomere-dysfunction induced foci (TIF) and  $\beta$ -galactosidase activity.** Procedures  
159 are described in supplemental Materials and Methods.

160 **In-gel G-overhang assay.** In-gel G-overhang assay was performed as described <sup>29</sup>, with minor  
161 modifications detailed in supplemental Materials and Methods.

162 **CRISPR/Cas9-mediated Apollo gene correction.** CRISPR/Cas9-mediated *Apollo* gene (*DCLRE1B*;  
163 Entrez Gene: 64858) correction procedure is detailed in supplemental Materials and Methods

164 **Expression Vectors.** Vectors are in supplemental Materials and Methods.

165 **Sister chromatid exchange detection (SCE).** SCE procedure is detailed in supplemental Materials  
166 and Methods.

167 **Western Blotting and coimmunoprecipitation.** Western Blotting, coimmunoprecipitation and  
168 antibodies are detailed in supplemental Materials and Methods

169 **Sensitivity to genotoxics assay.** Procedures to analyze the cellular sensitivity are detailed in

170 supplemental Materials and Methods.

171 **Statistical Analyses.** Statistics procedures are detailed in supplemental Materials and Methods.

172

173

174

175

176

177

178

179

180

181

182

183

184

185

186

187

188

189

190

191

192

193

194

195

196

197

198

199 **RESULTS**200 **Clinical features of patients**

201 We studied three unrelated families, each having a single child with clinical features evocative  
202 of IBMFS. Patient 1 (P1) is a 7-year-old Caucasian boy presenting growth retardation (-3 SD weight  
203 and height) and microcephaly (-2.5 SD) (**Table 1**). At the age of 4 months, laboratory tests, performed  
204 because of multiple petechiae, revealed a trilinear cytopenia. Bone marrow aspirate showed  
205 hypocellularity with rare megakaryocytes and moderate dyserythropoiesis. Immunological evaluation  
206 revealed profound B and NK cell lymphopenia. The proportions of recent thymus emigrant T  
207 lymphocytes and central memory T cells were reduced suggesting dysfunctional T lymphocyte  
208 homeostasis (**Supplemental Table 1**). The patient needed transfusion support with platelet and  
209 erythrocyte concentrates at the age of 11 months. He had undergone allogeneic hematopoietic stem  
210 cell transplantation (HSCT) at 15 months of age. Other clinical features included facial dysmorphia  
211 (hypotelorism), delayed speech, and esophageal strictures that appeared at the age of 5 years.

212 Patient 2 is an 11-year-old Portuguese girl born from consanguineous parents. Intrauterine  
213 growth retardation (IUGR) was diagnosed in the 3<sup>rd</sup> trimester. At birth, the patient was hypotrophic with  
214 weight at 1,685 g, height at 40.5 cm and head circumference of 31 cm (-2 SD) (**Table 1**). She  
215 presented with skin bruising and petechiae. Her hemogram revealed pancytopenia. A bone marrow  
216 aspirate revealed marked hypocellularity, reduced percentage of myeloid precursors, rare neutrophils  
217 with hyposegmented nuclei, and signs of dyserythropoiesis. Immunological evaluation showed a  
218 virtual absence of B and NK cells (**Supplemental Table 1**). She received transfusion support with  
219 platelet and erythrocyte concentrates. As severe progressive pancytopenia developed, allogeneic  
220 HSCT was successfully performed at 8 months of age. At 8 years of age she developed  
221 mucocutaneous features including hyperpigmented areas of the trunk and limbs, sparse scalp hair,  
222 leukoplakia, and dystrophic nails (**Supplemental Figure 1**).

223 Patient 3 is a 6-year-old Argentinian boy (**Table 1**) presenting with progressive bone marrow  
224 failure. His immunological evaluation evidenced profound B and NK cell lymphopenia (**Supplemental**  
225 **Table 1**). T lymphocyte count was normal but a slight reduction of recent thymus emigrant T  
226 lymphocytes was noted that was however not accompanied by a bias in T-cell repertoire, as inferred  
227 by T cell receptor gamma gene rearrangement analysis (**Supplemental Figure 2**)<sup>30</sup>. He receives

228 transfusion support (platelet and erythrocyte concentrates) and immunoglobulin replacement since the  
229 age of 3 months. He developed an inflammatory bowel disease at 10 months of age. Endoscopy  
230 showed a severe ulcerative pancolitis with signs of chronicity. Until now, the patient does not present  
231 any mucocutaneous or neurodevelopmental features.

232 Overall, the association of early-onset bone marrow failure, immunodeficiency, developmental  
233 defects and premature aging features in the 3 patients were consistent with DC/HH <sup>2-5</sup>.

234

### 235 **Patients exhibit normal global telomere length**

236 Since DC/HH are classically associated with abnormally short telomeres <sup>2,10</sup>, we assessed  
237 telomere length in patients. Surprisingly, telomere restriction fragment (TRF) analysis did not unveil a  
238 significant telomere length defect in patients' blood samples (obtained before HSCT) as compared to  
239 their parents (**Figure 1A**), and in contrast to HH patients with RTEL1 or PARN deficiency (**Figure 1B**)  
240 <sup>31-34</sup>. Flow-FISH <sup>10</sup> further confirmed the normal telomere length in blood cells from P1 and P3 (P2's  
241 blood sample before HSCT was not available) (**Figure 1C**). The telomere length in P1 and P3's blood  
242 cells sharply contrasted with the critically short telomeres measured in 13 DC/HH patients carrying  
243 pathogenic variants in TBD-causing genes (**Figure 1C**). Collectively, these results indicate that the 3  
244 patients, although presenting clinical features akin to DC/HH, did not exhibit critically short telomeres  
245 as classically observed in these diseases.

246 Subtle telomere instability resulting from rare sudden telomere loss that does not translate to  
247 global telomere shortening has been previously reported <sup>35</sup>. Telomere Shortest Length Assay (TeSLA),  
248 a highly sensitive method to detect the shortest telomeres <sup>28</sup>, highlighted a significant increase in the  
249 frequency of very short telomeres in P1's blood cells (**Figure 1D**). Thus, the combination of TeSLA  
250 analysis and telomere length measurement by TRF and Flow-FISH suggested telomere instability in  
251 patients' cells that does not translate into global telomere length reduction.

252

### 253 **Biallelic Apollo variants in patients**

254 To determine the molecular etiology of this atypical TBD we performed whole-exome  
255 sequencing in P1 and P3 and Haloplex targeted sequencing of 10 telomere-related genes in P2. This



256 analysis singled out *Apollo/DCLRE1B* as the only common gene carrying biallelic variants in the three  
257 patients. Sanger sequencing confirmed the *Apollo* variants which corresponded in P1 to a c.364C>T  
258 substitution leading to a premature stop codon (p.Arg122\*; NP\_073747.1) inherited from the healthy  
259 mother, and a c.426A>T substitution causing a p.Leu142Phe missense variant (thereafter noted  
260 L142F) inherited from the healthy father (**Figure 2A; Supplemental Figure 3**). P2 carried a  
261 homozygous *Apollo* missense variant that, as in P1, affected the amino-acid p.Leu142 but changing it  
262 towards a serine (c.425T>C; p.Leu142Ser, thereafter noted L142S). As expected in a context of  
263 consanguinity, both P2's healthy parents carried the c.425T>C; L142S variant at a heterozygous  
264 status (**Supplemental Figure 3**). P3 carried compound heterozygous *Apollo* variants consisting in a  
265 c.472C>T substitution producing a premature stop codon p.Arg158\* inherited from his healthy mother  
266 and, as in P2, a substitution c.425T>C; L142S inherited from her father (**Figure 2A; Supplemental**  
267 **Figure 3**).

268 The CADD<sup>36</sup> scores and the American College of Medical Genetics and Genomics  
269 standards<sup>37</sup> predicted the four *Apollo* variants to be deleterious/pathogenic. *Apollo* L142F and L142S  
270 variants were absent in gnomAD database, while both *Apollo* p.Arg122\* and p.Arg158\* variants were  
271 present at a very low frequency (**Supplemental Table 2**). Furthermore, according to gnomAD, loss-of-  
272 function (LOF) variant observed/expected ratio for *Apollo* is of 0.2, suggesting intolerance of LOF  
273 variants. Direct sequencing of *Apollo* cDNA from P1's fibroblasts detected the c.346C>T;p.R122\*  
274 variant indicating that it does not cause nonsense-mediated decay (NMD) (**Supplemental Figure 4**).  
275 However, because the low endogenous expression of *Apollo* precludes its detection by specific  
276 antibodies<sup>20,21</sup>, we could not test whether the c.346C>T;p.R122\* variant produces a severely truncated  
277 form of *Apollo*. P3's cells were not available to assess whether the c.472C>T; p.R158\* variant causes  
278 NMD.

279 *Apollo* belongs to the  $\beta$ -CASP family of proteins characterized by the presence of a specific  
280 clamp (the  $\beta$ -CASP domain) inserted into the  $\beta$ -lactamase domain and covering the nuclease active  
281 site<sup>38</sup>. The *Apollo* residue L142, located in the  $\beta$ -lactamase domain (**Figure 2B**), is highly conserved  
282 across species and in other  $\beta$ -CASP proteins (**Supplemental Figure 5**). *Apollo*'s 3D structure  
283 highlights that L142 participates in the hydrophobic core of the metallo- $\beta$ -lactamase domain (**Figure**  
284 **2C**). It is located nearby the conserved D145 residue (**Supplemental Figure 5**) that binds the amino

285 acid H276 that is believed to bind the phosphodiester cleaved by the nuclease<sup>39</sup>. L142F and L142S  
286 substitutions are thus predicted to indirectly impact the Apollo nuclease activity by structural  
287 disturbance nearby the active site.

288 Telomere localization of Apollo depends on the interaction of its TBM domain with the TRFH  
289 domain of TRF2<sup>20-22,24,26</sup>. To know whether the L142S and L142F variants could impact Apollo's  
290 stability/expression and/or its interaction with TRF2, we performed immunoblots and co-IP with  
291 extracts from HEK293T cells transfected with wild type (WT) or mutant FLAG-tagged Apollo-  
292 expressing vectors. The similar detection of WT and Apollo mutants indicated that the L142S and  
293 L142F variants did not modify the Apollo expression/stability, at least not in the context of  
294 overexpression (**Figure 2D**). However, a consistent reduced amount of endogenous TRF2 was co-  
295 immunoprecipitated with the Apollo mutants (**Figure 2D**) suggesting that, although at a distance from  
296 the TBM (**Figure 2B**), both variants partially impaired Apollo interaction with TRF2.

297 Altogether, these results indicate that the 3 patients carry biallelic variants in *Apollo*. At least  
298 one allele in each patient corresponds to a missense variant affecting the amino acid L142 that does  
299 not impact Apollo expression/stability but partially reduces its capacity to interact with TRF2 and is  
300 predicted to impact the catalytic activity of Apollo.

301

### 302 **Patients' cells exhibit some telomere aberrations but not global telomere shortening**

303 To examine the functional consequences of Apollo variants on telomere stability we analyzed  
304 the phenotype of primary fibroblasts obtained from P1 and P2. TRF analysis did not reveal abnormal  
305 telomere length in patients' primary fibroblasts (**Figure 3A**), an observation congruent with the results  
306 obtained in patients' blood cells (**Figure 1**). Furthermore, unlike primary fibroblasts from TBDs patients  
307 with short telomeres (e.g. RTEL1-, TIN2- and PARN-deficient fibroblasts<sup>31,33,34,40</sup>), or even RTEL1-  
308 deficient patient's primary fibroblasts with normal telomere length<sup>41</sup>, P1 and P2's primary fibroblasts  
309 did not exhibit an increase in telomere dysfunction-induced foci (TIFs)<sup>42,43</sup> and senescence-  
310 associated  $\beta$ -galactosidase activity (**Supplemental Figures 6A-B**) suggesting that telomeres in  
311 patients' fibroblasts are not overwhelmingly deprotected. Next, TeSLA performed in patients' primary  
312 fibroblasts uncovered a slight increase in the frequency of very short telomeres that was however not  
313 statistically significant (**Supplemental Figure 6C**). Even though we precisely quantified the input DNA

314 used for TeSLA analysis, we consistently noticed a reduction of the number of bands (corresponding  
315 to PCR-amplified products) in samples from both patients' fibroblasts compared to controls  
316 (**Supplemental Figure 6C**). Since TeSLA depends on annealing of a primer to the telomeric G-  
317 overhang<sup>28</sup>, this suggested a reduced availability of G-overhang in patients' cells, which would be in  
318 accordance with the role of Apollo in the generation of G-overhang from the leading telomere  
319 described in murine models<sup>24-26</sup>. In-gel hybridization assays confirmed an overall reduction of 30-50%  
320 of the G-overhang in patients' cells (**Supplemental Figure 6D**). Since the calculated G-overhang  
321 value corresponds to the portion of the telomere that is single stranded, we also corrected for the  
322 effect of the telomere length by multiplying the native/denatured signal by the mean TRF length (MTL).  
323 Also these values, reflecting the absolute G-overhang length, were reduced as compared to the WT  
324 controls (**Supplemental Figure 6D**, experiment #3). We next performed telomeric FISH on  
325 metaphase spreads of SV40-transformed fibroblasts to detect putative telomere aberrations (**Figure**  
326 **3B**). P1 and P2 patients' cells exhibited a slight but significant increase of telomere-telomere fusions.  
327 P2's fibroblasts also had a statistically significant increase of MTS reflecting telomere fragility<sup>44</sup>, while  
328 P1's cells exhibited a significant, although moderate, increase of dicentric chromosomes and sister  
329 chromatid fusions (**Figure 3B-C**). Other telomere aberrations were not overrepresented in patients'  
330 cells.

331 We concluded from these analyses that the Apollo-mutated patients' cells exhibit some signs  
332 of telomere instability and reduced G-overhang that are not associated with global telomere shortening  
333 and hallmarks of dysfunctional telomeres (*i.e.*, TIFs and senescence), a situation different from the  
334 one observed in classical TBDs<sup>31,33,34,40,45</sup>.

335

### 336 **Chromosome instability and DNA repair defect in patients' cells**

337 Next, we assessed whether patients' Apollo-deficient cells could exhibit genome instability and  
338 impaired DNA repair. Metaphase spreads in patients' SV40-transformed fibroblasts highlighted a  
339 significant increase in spontaneous radial chromosomes (**Figure 4A-B**), which represent  
340 intermediates of recombination associated with genomic instability. The frequency of radial  
341 chromosomes was further increased in MMC-treated patients' cells treated (**Figure 4B**). As compared

342 to WT cells, MMC-patients' cells also showed a significant increase in chromosome breaks (**Figure**  
343 **4A-C**) and sister chromatid exchanges (**Supplemental Figure 7**), suggesting a defect in ICL-repair.  
344 The reduced cell survival of MMC-treated patients' Apollo-mutated fibroblasts confirmed an impaired  
345 ICL repair, which was however not as pronounced as cells from a FA patient (**Figure 4D**), and not  
346 associated with defective FANCD2 ubiquitination (**Supplemental Figure 8**). The DNA repair defect  
347 was not restricted to ICL since P1 and P2's fibroblasts also exhibited an increased sensitivity to  
348 aphidicolin that causes replicative stress by inhibiting DNA polymerase (**Figure 4E**), as well as to  
349 phleomycin, a DNA double-strand break-inducer (**Figure 4F**). These results indicate that DNA repair  
350 of several distinct DNA injuries is impaired in patients' Apollo-mutated cells.

351 Next, we used CRISPR/Cas9-mediated homology-directed repair to correct the homozygous  
352 L142S Apollo variant by a WT sequence in P2's hTERT-immortalized SV40-fibroblasts. We obtained a  
353 P2's SV40-hTERT cellular clone carrying a WT *Apollo* sequence in one allele, therefore corresponding  
354 to a heterozygous carrier of the L142S Apollo variant (noted P2<sup>L142S/WT</sup>; **Figure 4G**; **Supplemental Fig.**  
355 **9**). While the native P2's clone with the homozygous L142S Apollo variant (noted P2<sup>L142S/L142S</sup>)  
356 exhibited reduced cell survival upon phleomycin treatment, P2<sup>L142S/WT</sup> cells behaved similarly to WT  
357 cells (**Figure 4H**). This result provides evidence of a causal link between impaired DNA repair and the  
358 presence of biallelic *Apollo* variants in patients' cells.

359 Collectively, our results indicate that the biallelic *Apollo* variants identified in patients cause  
360 telomere fragility, spontaneous genomic instability, and impaired DNA repair.

361

### 362 **Telomere phenotype in human Apollo KO cell lines**

363 The complete loss-of-function of Apollo is embryonic lethal in mouse<sup>24,26,46</sup> and Apollo KO  
364 MEFs exhibit sharp telomere abnormalities, mostly characterized by leading telomere fusions<sup>24,26,46</sup>.  
365 This severe phenotype contrasts with the rather limited telomere defect observed in patients' cells. We  
366 thus asked whether a complete lack of Apollo in human cell lines could have a stronger impact on  
367 telomere stability than the one found in patients' cells. We generated two HT1080 Apollo KO cell lines  
368 (#1 and #2) by using CRISPR/Cas9 with two distinct RNA guides (**Supplemental Figure 10**). Unlike  
369 patients' cells, HT1080 Apollo KO cell lines exhibited telomere dysfunction as inferred by the  
370 significant increase in TIFs (**Figure 5A**). In addition, both HT1080 Apollo KO cell lines exhibited a

371 significant augmentation of telomere-telomere fusion and dicentric chromosomes (**Figure 5B**), while  
372 other aberrations was not augmented (data not shown). Furthermore, TeSLA pointed out a significant  
373 increase in very short telomeres in Apollo KO cell lines (**Figure 5C**) and, as observed in primary  
374 fibroblasts from patients, a reduced number of bands amplified by TeSLA, suggesting defects in G-  
375 overhang formation (**Figure 5C; Supplemental Figure 6C**). Accordingly, in-gel hybridization  
376 highlighted a ~50% reduction of the relative G-overhang signal in the HT1080 Apollo KO cell line #1  
377 (**Figure 5D**). Strikingly, in-gel G-overhang assay also highlighted a sharp reduction of global telomere  
378 length in the Apollo KO cell line (**Figure 5D**). Correction for the effect of the global telomere length  
379 resulted in even a greater reduction in the absolute overhang length to 17% of the WT control (**Figure**  
380 **5D**). The assessment of global telomere length by Southern analysis of TRF confirmed that both  
381 HT1080 Apollo KO cell lines exhibit critically short telomeres as compared to a WT HT1080 cellular  
382 clone at a similar passage (**Figure 5E**).

383 Collectively, these analyses reveal that the complete loss-of-function of Apollo in human cells  
384 leads to a marked telomere phenotype more severe than the one observed in Apollo-deficient patients'  
385 cells. This result supports the idea that the Apollo L142F and L142S missense variants found in  
386 patients are hypomorphic.

387  
388  
389  
390  
391  
392  
393  
394  
395  
396  
397  
398  
399

400 **DISCUSSION**

401           Herein we provide evidence that biallelic variants in *Apollo* cause a severe form of IBMFS  
402 characterized by early onset bone marrow failure, immunodeficiency (mostly B and NK lymphopenia),  
403 mucocutaneous anomalies, and several developmental defects (including microcephaly and  
404 intrauterine growth retardation). These clinical features are indistinguishable from the telomere biology  
405 disorders DC and HH<sup>2,3</sup>. Remarkably, however, unlike patients with classical DC/HH, cells from  
406 *Apollo*-deficient patients did not exhibit excessive overall telomere shortening. This finding defines  
407 biallelic variants in *Apollo* as a cause of a hitherto unrecognized IBMFS, which shares many hallmarks  
408 with DC/HH but is distinguished by normal overall telomere length. Since telomere length  
409 measurement represents an accurate and reliable mean to diagnose short telomere syndromes<sup>10</sup>, we  
410 propose that *Apollo* should be considered as a candidate gene in patients presenting clinical features  
411 of TBDs but normal telomere length. Since DC/HH are cancer-prone diseases<sup>2,47-49</sup>, *Apollo* patients  
412 might be at risk to develop cancer. Furthermore, heterozygous carriers of variants in classical TBD-  
413 causing genes are predisposed to prematurely develop fibrosis and other age-related ailments<sup>2,50,51</sup>.  
414 The *Apollo*-deficient patients' parents, who are heterozygous carriers of *Apollo* variants, are still young  
415 and healthy so far. A careful attention should be paid to ensure that they would not prematurely  
416 develop age-related diseases.

417           Consistent with the reported role of *Apollo* in DNA repair<sup>13</sup>, we showed that patients' *Apollo*-  
418 deficient fibroblasts exhibited spontaneous chromosome anomalies, impaired repair of ICL and DSBs,  
419 and increased sensitivity to replicative stress. Importantly, CRISPR/Cas9-mediated correction of one  
420 *Apollo*-mutated allele complemented the DNA repair defect in P2's cells, demonstrating the causal link  
421 between *Apollo* deficiency and impaired DNA repair in these cells. Notably, we noticed that patients'  
422 *Apollo*-deficient cells shared several features with cells from FA patients, including increased  
423 frequency of radial chromosomes and defective ICL repair. These observations, congruent with  
424 previous studies conducted in *Apollo*-depleted human cells, support the idea that *Apollo* functions in  
425 the FA pathway<sup>14,15,52</sup>. The normal FANCD2 ubiquitination in MMC-treated *Apollo*-deficient cells  
426 suggests that *Apollo* functions downstream of this step in the FA/BRCA pathway as previously  
427 suggested in *Apollo*-depleted cells<sup>12,14</sup>. However, the extremely severe phenotype of *Apollo*-deficient  
428 patients (requiring HSCT before the age of 18 months in two of them) contrasted with the progressive

429 bone marrow failure usually detected between 5 - 10 years of age in FA patients <sup>1</sup>. Furthermore, unlike  
430 blood cells from FA patients <sup>53</sup>, blood lymphocytes from the three Apollo-deficient patients did not  
431 exhibit increased chromosomal breakages in the presence of the ICL-inducer diepoxybutane (**Table**  
432 **1**). Interestingly, sensitivity to ICL-inducer restricted to fibroblasts but not to blood cells has also been  
433 observed in RTEL1-deficient HH patients <sup>54,55</sup>, raising the possibility that RTEL1 and Apollo may  
434 participate in a common DNA repair pathway. Together, these observations rule out a diagnosis of  
435 Fanconi anemia in Apollo-deficient patients and suggest that Apollo-deficiency causes defects in  
436 biological processes that differ from and expand beyond the classical FA/BRCA pathway.

437         Recently, Mendez-Bermudez and colleagues have proposed that some factors originally  
438 devoted to warrant proper DNA replication and repair have evolved to be recruited and act at  
439 telomeres <sup>56</sup>. Interestingly, phylogenetic analyses suggested that Apollo might be one of these factors  
440 since its TBM domain coemerged with the two telomeric paralogues TRF1 and TRF2, presumably to  
441 direct the specific binding of Apollo to TRF2 <sup>27,57</sup>. The importance of the interaction between Apollo  
442 and TRF2 has been further substantiated by a comparative genomic analysis that pinpointed the  
443 existence of variants in the TBM of Apollo and in the TRFH domain of TRF2 in long-lived Galapagos  
444 giant tortoises compared to short-lived turtles <sup>58</sup>. This finding argues that variation in the strength of  
445 TRF2-Apollo interaction could influence aging and organismal lifespan. The fact that both missense  
446 Apollo variants L142S and L142F reduce the interaction with TRF2 supports the notion that they might  
447 contribute to the premature aging phenotype observed in patients. Furthermore, the decreased  
448 interaction between TRF2 and the Apollo L142S and L142F mutants suggests that the  $\beta$ -lactamase  
449 domain containing the L142 residue might possess a second interface that stabilizes the TBM-  
450 dependent Apollo-TRF2 interaction. This hypothesis will require further investigations.

451         Studies conducted in Apollo KO MEFs established that the nuclease activity of Apollo  
452 participated in the generation of the 3' G-overhang of the leading telomere <sup>24-26</sup>. The 30-50% reduction  
453 of G-overhang signal observed in Apollo-deficient patients' cells was similar to the one found in Apollo  
454 KO MEFs, supporting the idea that the patients' variants impair Apollo nuclease activity. However,  
455 several clues suggest that the L142S and L142F Apollo are hypomorphic rather than complete loss-of-  
456 function mutants. First, Apollo KO mice are unviable <sup>24,26,46</sup> and none of the three patients carry  
457 biallelic null *Apollo* alleles, but all carry at least one missense Apollo variant affecting the residue

458 L142. Furthermore, we noticed that the frequency of telomere fusions in Apollo-deficient patient cells  
459 was less pronounced than Apollo KO MEFs. Along the same line, other telomere anomalies detected  
460 in patients' cells were not accompanied by an increase in TIFs and premature senescence, in contrast  
461 to Apollo KO MEFs<sup>20,21,24,26</sup>. Lastly, human Apollo KO HT1080 cell lines exhibit a more pronounced  
462 telomere phenotype than patients' cells. In particular, the telomerase positive Apollo KO human  
463 HT1080 cell lines exhibited a severe telomere length defect contrasting with the normal telomere  
464 length measured in patients' Apollo-deficient cells. This raises the possibility that the critically short  
465 telomeres caused by the absence of Apollo could result from the high frequency of sudden telomere  
466 loss detected by TeSLA and/or uncontrolled telomere degradation by undetermined nuclease that  
467 could not be compensated by telomerase activity. Alternatively, one cannot exclude that Apollo  
468 contributes to the recruitment and/or activity of telomerase to telomeres. In these two last hypotheses  
469 we assume that the presence of Apollo at telomeres, even at a low level (e.g. in depleted cells by  
470 siRNA/shRNA) or with defective nuclease activity, would suffice to warrant telomere maintenance and  
471 partial telomere protection. This surmise is further supported by the observation that a nuclease-dead  
472 Apollo mutant expressed in Apollo KO MEFs exhibit a telomeric protective effect despite an impaired  
473 G-overhang generation at leading telomeres<sup>26</sup>. Collectively, these findings led us to propose that the  
474 L142F and L142S Apollo mutants, although deleterious, retain some protective function compatible  
475 with life. Future studies will be necessary to further determine the structural and functional impact of  
476 the L142F and L142S Apollo variants and figure out what governs the phenotypic differences between  
477 patients' Apollo-deficient cells and murine and human Apollo KO cell lines.

478 We conclude from this study that biallelic *Apollo* variants leading to both impaired DNA repair  
479 and telomere instability are responsible for a hitherto unrecognized IBMFS akin to Høyeraal-  
480 Hreidarsson syndrome that is however not associated with excessive telomere shortening. These  
481 findings define Apollo as a genome caretaker critical for the proper development of the immuno-  
482 hematological system in humans.

483

484

485



486 **Acknowledgements:** Authors thank the individuals P1, P2, and P3 and their families for their  
487 contribution in this study. P.R. thanks Yanick Crow for the kind gift of Bloom-deficient SV40-  
488 transformed fibroblasts<sup>59</sup>. This work has been supported by institutional grants from INSERM, Ligue  
489 Nationale contre le Cancer (Equipe Labellisée La Ligue 'LIGUE 2020' to P.R. and 'LIGUE 2021' to  
490 V.G.), CEREDIH (Centre de Référence Déficits Immunitaires Héritaires) and state funding from the  
491 Agence Nationale de la Recherche under "Investissements d'avenir" program (ANR-10-IAHU-01) and  
492 (ANR-21-CE12-APOthesis). This work was supported by the Israel Science Foundation grant  
493 [2071/18] to Y.T. and the Israel Ministry of Science and Technology (Navon Fellowship) to A.A. This  
494 work was also supported by the STEP-GTP Fellowship to A.A. and by the Israel-UK-Palestine  
495 GROWTH Fellowship Scheme, the British Council, to R.S. This study contributes to the IdEx  
496 Université de Paris ANR-18-IDEX-0001PR. P.R. is a scientist from the Centre National de la  
497 Recherche Scientifique (CNRS).

498  
499 **Authorship contributions.** L.K. carried out most of the experimental work. D.C. performed TeSLA  
500 analysis. A.A. and R.S. performed in-gel hybridization experiments. L.R. participated to the initial  
501 characterization of the shortest telomeres. P.R., C.K., S.D. and G.S. performed genetic analysis and  
502 identified *Apollo* variants. S. A-B., S.H., E.C., M.O., F.T., S.D., and G.S. identified the affected patients  
503 and assisted with related clinical and laboratory studies. E.L. performed Flow-FISH. M.M. provided  
504 intellectual input. C.A. performed TCR repertoire analysis. I.C. performed structural analysis. P.R.  
505 conceived the project and wrote the manuscript with editing contributions from J-P.V., F.T., I.C., V.G.,  
506 and Y.T.

507

#### 508 **Disclosure of conflicts of interests**

509 The authors declare no competing interests.

510

511

512

513

## 514 REFERENCES

- 515 1. Savage SA, Dufour C. Classical inherited bone marrow failure syndromes with high risk for  
516 myelodysplastic syndrome and acute myelogenous leukemia. *Semin Hematol.* 2017;54(2):105-114.
- 517 2. Savage SA. Beginning at the ends: telomeres and human disease. *F1000Res.* 2018;7.
- 518 3. Glousker G, Touzot F, Revy P, Tzfati Y, Savage SA. Unraveling the pathogenesis of Hoyeraal-  
519 Hreidarsson syndrome, a complex telomere biology disorder. *Br J Haematol.* 2015.
- 520 4. Armanios M, Blackburn EH. The telomere syndromes. *Nat Rev Genet.* 2012;13(10):693-704.
- 521 5. Calado RT, Young NS. Telomere diseases. *N Engl J Med.* 2009;361(24):2353-2365.
- 522 6. de Lange T. Shelterin-Mediated Telomere Protection. *Annu Rev Genet.* 2018.
- 523 7. MacNeil DE, Bensoussan HJ, Autexier C. Telomerase Regulation from Beginning to the End. *Genes*  
524 *(Basel).* 2016;7(9).
- 525 8. Benyelles M, O'Donohue MF, Kermasson L, et al. NHP2 deficiency impairs rRNA biogenesis and  
526 causes pulmonary fibrosis and Hoyeraal-Hreidarsson syndrome. *Hum Mol Genet.* 2020;29(6):907-922.
- 527 9. Hao LY, Armanios M, Strong MA, et al. Short telomeres, even in the presence of telomerase, limit  
528 tissue renewal capacity. *Cell.* 2005;123(6):1121-1131.
- 529 10. Alder JK, Hanumanthu VS, Strong MA, et al. Diagnostic utility of telomere length testing in a hospital-  
530 based setting. *Proc Natl Acad Sci U S A.* 2018;115(10):E2358-E2365.
- 531 11. Alter BP, Rosenberg PS, Giri N, Baerlocher GM, Lansdorp PM, Savage SA. Telomere length is  
532 associated with disease severity and declines with age in dyskeratosis congenita. *Haematologica.* 2011.
- 533 12. Demuth I, Digweed M, Concannon P. Human SNM1B is required for normal cellular response to both  
534 DNA interstrand crosslink-inducing agents and ionizing radiation. *Oncogene.* 2004;23(53):8611-8618.
- 535 13. Schmiester M, Demuth I. SNM1B/Apollo in the DNA damage response and telomere maintenance.  
536 *Oncotarget.* 2017;8(29):48398-48409.
- 537 14. Bae JB, Mukhopadhyay SS, Liu L, et al. Snm1B/Apollo mediates replication fork collapse and S Phase  
538 checkpoint activation in response to DNA interstrand cross-links. *Oncogene.* 2008;27(37):5045-5056.
- 539 15. Demuth I, Bradshaw PS, Lindner A, et al. Endogenous hSNM1B/Apollo interacts with TRF2 and  
540 stimulates ATM in response to ionizing radiation. *DNA Repair (Amst).* 2008;7(8):1192-1201.
- 541 16. Mason JM, Das I, Arlt M, et al. The SNM1B/APOLLO DNA nuclease functions in resolution of  
542 replication stress and maintenance of common fragile site stability. *Hum Mol Genet.* 2013;22(24):4901-4913.
- 543 17. Mason JM, Sekiguchi JM. Snm1B/Apollo functions in the Fanconi anemia pathway in response to DNA  
544 interstrand crosslinks. *Hum Mol Genet.* 2011;20(13):2549-2559.
- 545 18. Michailidou K, Hall P, Gonzalez-Neira A, et al. Large-scale genotyping identifies 41 new loci  
546 associated with breast cancer risk. *Nat Genet.* 2013;45(4):353-361, 361e351-352.
- 547 19. Liang XS, Pfeiffer RM, Wheeler W, et al. Genetic variants in DNA repair genes and the risk of  
548 cutaneous malignant melanoma in melanoma-prone families with/without CDKN2A mutations. *International*  
549 *Journal of Cancer.* 2012;130(9):2062-2066.
- 550 20. Lenain C, Bauwens S, Amiard S, Brunori M, Giraud-Panis MJ, Gilson E. The Apollo 5' exonuclease  
551 functions together with TRF2 to protect telomeres from DNA repair. *Curr Biol.* 2006;16(13):1303-1310.
- 552 21. van Overbeek M, de Lange T. Apollo, an Artemis-related nuclease, interacts with TRF2 and protects  
553 human telomeres in S phase. *Curr Biol.* 2006;16(13):1295-1302.
- 554 22. Freibaum BD, Counter CM. hSnm1B is a novel telomere-associated protein. *J Biol Chem.*  
555 2006;281(22):15033-15036.
- 556 23. Ye J, Lenain C, Bauwens S, et al. TRF2 and apollo cooperate with topoisomerase 2alpha to protect  
557 human telomeres from replicative damage. *Cell.* 2010;142(2):230-242.
- 558 24. Lam YC, Akhter S, Gu P, et al. SNM1B/Apollo protects leading-strand telomeres against NHEJ-  
559 mediated repair. *Embo J.* 2010;29(13):2230-2241.
- 560 25. Wu P, Takai H, de Lange T. Telomeric 3' overhangs derive from resection by Exo1 and Apollo and fill-  
561 in by POT1b-associated CST. *Cell.* 2012;150(1):39-52.
- 562 26. Wu P, van Overbeek M, Rooney S, de Lange T. Apollo contributes to G overhang maintenance and  
563 protects leading-end telomeres. *Mol Cell.* 2010;39(4):606-617.
- 564 27. Touzot F, Callebaut I, Soulier J, et al. Function of Apollo (SNM1B) at telomere highlighted by a splice  
565 variant identified in a patient with Hoyeraal-Hreidarsson syndrome. *Proc Natl Acad Sci U S A.*  
566 2010;107(22):10097-10102.
- 567 28. Lai TP, Zhang N, Noh J, et al. A method for measuring the distribution of the shortest telomeres in cells  
568 and tissues. *Nat Commun.* 2017;8(1):1356.
- 569 29. Awad A, Glousker G, Lamm N, et al. Full length RTEL1 is required for the elongation of the single-  
570 stranded telomeric overhang by telomerase. *Nucleic Acids Res.* 2020;48(13):7239-7251.

- 571 30. Armand M, Derrioux C, Beldjord K, et al. A New and Simple TRG Multiplex PCR Assay for  
572 Assessment of T-cell Clonality: A Comparative Study from the EuroClonality Consortium. *Hemasphere*.  
573 2019;3(3):e255.
- 574 31. Benyelles M, Episkopou H, O'Donohue MF, et al. Impaired telomere integrity and rRNA biogenesis in  
575 PARN-deficient patients and knock-out models. *EMBO Mol Med*. 2019;11(7):e10201.
- 576 32. Touzot F, Kermasson L, Jullien L, et al. Extended Clinical and Genetic Spectrum Associated with  
577 Biallelic RTEL1 Mutations. *Blood Advances*. 2016;1(1).
- 578 33. Le Guen T, Jullien L, Touzot F, et al. Human RTEL1 deficiency causes Hoyeraal-Hreidarsson  
579 syndrome with short telomeres and genome instability. *Hum Mol Genet*. 2013;22(16):3239-3249.
- 580 34. Jullien L, Kannengiesser C, Kermasson L, et al. Mutations of the RTEL1 Helicase in a Hoyeraal-  
581 Hreidarsson Syndrome Patient Highlight the Importance of the ARCH Domain. *Hum Mutat*. 2016;37(5):469-  
582 472.
- 583 35. Takai H, Jenkinson E, Kabir S, et al. A POT1 mutation implicates defective telomere end fill-in and  
584 telomere truncations in Coats plus. *Genes Dev*. 2016;30(7):812-826.
- 585 36. Kircher M, Witten DM, Jain P, O'Roak BJ, Cooper GM, Shendure J. A general framework for  
586 estimating the relative pathogenicity of human genetic variants. *Nat Genet*. 2014;46(3):310-315.
- 587 37. Richards S, Aziz N, Bale S, et al. Standards and guidelines for the interpretation of sequence variants: a  
588 joint consensus recommendation of the American College of Medical Genetics and Genomics and the  
589 Association for Molecular Pathology. *Genet Med*. 2015;17(5):405-424.
- 590 38. Callebaut I, Moshous D, Mornon JP, de Villartay JP. Metallo-beta-lactamase fold within nucleic acids  
591 processing enzymes: the beta-CASP family. *Nucleic Acids Res*. 2002;30(16):3592-3601.
- 592 39. Allerston CK, Lee SY, Newman JA, Schofield CJ, McHugh PJ, Gileadi O. The structures of the  
593 SNM1A and SNM1B/Apollo nuclease domains reveal a potential basis for their distinct DNA processing  
594 activities. *Nucleic Acids Res*. 2015;43(22):11047-11060.
- 595 40. Touzot F, Gaillard L, Vasquez N, et al. Heterogeneous telomere defects in patients with severe forms of  
596 dyskeratosis congenita. *J Allergy Clin Immunol*. 2012;129(2):473-482, 482 e471-473.
- 597 41. Lamm N, Ordan E, Shponkin R, Richler C, Aker M, Tzfati Y. Diminished telomeric 3' overhangs are  
598 associated with telomere dysfunction in Hoyeraal-Hreidarsson syndrome. *PLoS One*. 2009;4(5):e5666.
- 599 42. Takai H, Smogorzewska A, de Lange T. DNA damage foci at dysfunctional telomeres. *Curr Biol*.  
600 2003;13(17):1549-1556.
- 601 43. d'Adda di Fagagna F, Reaper PM, Clay-Farrace L, et al. A DNA damage checkpoint response in  
602 telomere-initiated senescence. *Nature*. 2003;426(6963):194-198.
- 603 44. Sfeir A, Kosiyatrakul ST, Hockemeyer D, et al. Mammalian telomeres resemble fragile sites and require  
604 TRF1 for efficient replication. *Cell*. 2009;138(1):90-103.
- 605 45. Deng Z, Glousker G, Molczan A, et al. Inherited mutations in the helicase RTEL1 cause telomere  
606 dysfunction and Hoyeraal-Hreidarsson syndrome. *Proc Natl Acad Sci U S A*. 2013;110(36):E3408-3416.
- 607 46. Akhter S, Lam YC, Chang S, Legerski RJ. The telomeric protein SNM1B/Apollo is required for normal  
608 cell proliferation and embryonic development. *Aging Cell*. 2010;9(6):1047-1056.
- 609 47. Alter BP, Giri N, Savage SA, Rosenberg PS. Cancer in dyskeratosis congenita. *Blood*.  
610 2009;113(26):6549-6557.
- 611 48. Schratz KE, Haley L, Danoff SK, et al. Cancer spectrum and outcomes in the Mendelian short telomere  
612 syndromes. *Blood*. 2020;135(22):1946-1956.
- 613 49. Stanley SE, Armanios M. The short and long telomere syndromes: paired paradigms for molecular  
614 medicine. *Curr Opin Genet Dev*. 2015;33:1-9.
- 615 50. Garcia CK. Insights from human genetic studies of lung and organ fibrosis. *J Clin Invest*.  
616 2018;128(1):36-44.
- 617 51. Juge PA, Borie R, Kannengiesser C, et al. Shared genetic predisposition in rheumatoid arthritis-  
618 interstitial lung disease and familial pulmonary fibrosis. *Eur Respir J*. 2017;49(5).
- 619 52. Salewsky B, Schmiester M, Schindler D, Digweed M, Demuth I. The nuclease hSNM1B/Apollo is  
620 linked to the Fanconi anemia pathway via its interaction with FANCP/SLX4. *Hum Mol Genet*.  
621 2012;21(22):4948-4956.
- 622 53. Auerbach AD. Fanconi anemia and its diagnosis. *Mutat Res*. 2009;668(1-2):4-10.
- 623 54. Speckmann C, Sahoo SS, Rizzi M, et al. Clinical and Molecular Heterogeneity of RTEL1 Deficiency.  
624 *Front Immunol*. 2017;8:449.
- 625 55. Walne AJ, Vulliamy T, Kirwan M, Plagnol V, Dokal I. Constitutional mutations in RTEL1 cause severe  
626 dyskeratosis congenita. *Am J Hum Genet*. 2013;92(3):448-453.
- 627 56. Mendez-Bermudez A, Giraud-Panis MJ, Ye J, Gilson E. Heterochromatin replication goes hand in hand  
628 with telomere protection. *Nat Struct Mol Biol*. 2020;27(4):313-318.

- 629 57. Myler LR, Kinzig CG, Sasi NK, Zakusilo G, Cai SW, de Lange T. The evolution of metazoan shelterin.  
630 *Genes Dev.* 2021.
- 631 58. Quesada V, Freitas-Rodriguez S, Miller J, et al. Giant tortoise genomes provide insights into longevity  
632 and age-related disease. *Nat Ecol Evol.* 2019;3(1):87-95.
- 633 59. Gratia M, Rodero MP, Conrad C, et al. Bloom syndrome protein restrains innate immune sensing of  
634 micronuclei by cGAS. *J Exp Med.* 2019;216(5):1199-1213.
- 635 60. Buck D, Malivert L, de Chasseval R, et al. Cernunnos, a novel nonhomologous end-joining factor, is  
636 mutated in human immunodeficiency with microcephaly. *Cell.* 2006;124(2):287-299.  
637
- 638
- 639
- 640
- 641
- 642
- 643
- 644
- 645
- 646
- 647
- 648
- 649
- 650
- 651
- 652
- 653
- 654
- 655
- 656
- 657
- 658
- 659
- 660
- 661

## 662 TABLES

663

664 Table 1. Clinical features of patients

	Patient 1 (P1)	Patient 2 (P2)	Patient 3 (P3)
Sex	Male	Female	Male
Consanguinity	No	Yes	No
Ethnicity	French/Caucasian	Portuguese	Argentinian
Developmental features			
IUGR	No	Yes, <3rd percentile	No
Prematurity	No	Yes (36 WG)	No
Microcephaly	Yes (<2 SD)	Yes (<2 SD)	No
Dysmorphism	Yes (hypotelorism)	Yes	No
Hypocellular bone marrow failure	Yes, at 4 months	Yes, at birth	Yes, at 3 months
Immunodeficiency	Yes	Yes	Yes
Neurological features			
Developmental delay	Speech delay	Mild learning difficulties	No
Cerebellar atrophy	No	No	No
Gastrointestinal features	Esophageal strictures	Esophageal strictures	Inflammatory colitis
Mucocutaneous features			
	None	Oral leukoplakia Nail dystrophy Skin hyperpigmentation	None
Increased DEB-induced chromosome breaks in blood cells	No	No	No
Outcome	HSCT at 15 months, alive	HSCT at 3 months, alive	Alive, under transfusion support and Ig replacement
HSCT conditioning regimens	Fludarabine, Busulfan, ATG	Fludarabine, Cyclophosphamide, ATG	NA
Toxicity	No	Cutaneous GVHD	NA

665

666 IUGR: Intrauterine growth retardation; SD: Standard deviation; DEB: Diepoxybutane; HSCT:  
667 Hematopoietic stem cell transplantation; ATG: Anti-thymocyte globulin; GVHD: Graft versus host  
668 disease; WG: Weeks of gestation; DEB: Diepoxybutane; HSCT: Hematopoietic stem cell  
669 transplantation; NA: Not applicable.

670

671

672

673

674

675

676

677

678

679

680

681

682 **Figure legends.**

683 **Figure 1: Telomere length in blood cells from patients.** (A) Telomere length determined by  
684 telomere restriction fragment (TRF) assay in DNA from blood cells from patients P1, P2, P3 and their  
685 parents (P3's father sample was not available). (B) Graphic representation of TRF data obtained in (A)  
686 as well as in 8 age-matched controls, 8 RTEL1-deficient patients, and 2 PARN-deficient patients  
687 described in<sup>31-34</sup>. (C) Relative telomere length in comparison with the tetraploid control cell line (1301)  
688 measured by Flow FISH in blood cells from P1, P3, P3's mother and 13 DC/HHS patients with variants  
689 in DKC1, TERT, TERC, RTEL1 or TINF2. Lines represent the 1st, 10th, 50th and 90th percentiles of  
690 telomere length of healthy controls. (D) (Left) Detection of the shortest telomeres by TeSLA performed  
691 in blood cells from P1 and an age-matched healthy donor. (Right) Graphic representation of TeSLA  
692 data with statistical analyses reveals a significant increase in telomere loss events in P1's blood  
693 sample. A two-tailed student t-test was used for statistical analyses of band size and a  $\chi^2$  test was  
694 used for analysis of fraction <1.5kb.

695

696 **Figure 2. Genetic analysis identified Apollo variants in the patients.** (A) Pedigrees and Apollo  
697 variants identified in individuals P1, P2 and P3 by Sanger sequencing. (B) Domain architecture of the  
698 human Apollo with the localization of the identified variants of P1, P2 and P3. NLS: nuclear localization  
699 signal; TBM: TRFH binding motif. (C) Ribbon representation of the 3D structure of human Apollo  
700 catalytic domain (pdb 5AHO,<sup>39</sup> with two coordinated zinc ions and two tartrate molecules at the active  
701 site. Details of the region surrounding L142 are given in the box at left, highlighting the hydrophobic  
702 core in which L142 participates, in the vicinity of motif A D145 (bond with motif B H247, itself bound to  
703 a tartrate molecule, which may represent the phosphodiester cleaved by the nuclease<sup>39</sup>). (D) Co-  
704 immunoprecipitation of endogenous TRF2 with WT or mutated forms of FLAG-Apollo. Picture  
705 representative of three independent experiments.

706

707 **Figure 3. Telomere phenotype in patients' fibroblasts.** (A) Telomere length determined by TRF in  
708 primary fibroblasts from two healthy controls and patients P1 and P2. Population doubling is indicated  
709 in brackets. (B) Representative pictures of normal chromosomes and chromosomes with the indicated  
710 telomeric aberrations detected by FISH. (C) Quantitative analysis of telomeric aberrations detected by  
711 FISH in SV40-transformed fibroblasts from two age-matched healthy controls and P1 and P2 at similar  
712 passages (from passage 3 to 8). Ctl1 fibroblasts are from a healthy male individual, and Ctl2 are from  
713 a healthy female individual). Results from 5 independent experiments for P1 and 2 for P2 (Counted  
714 chromosomes: Ctl1:  $n = 1,945$ ; Ctl2:  $n = 1,462$ ; P1:  $n = 3,325$ ; P2:  $n = 2,631$ ) Averages are shown and  
715 chi-square tests were applied to compare Ctls with either P1 or P2.

716

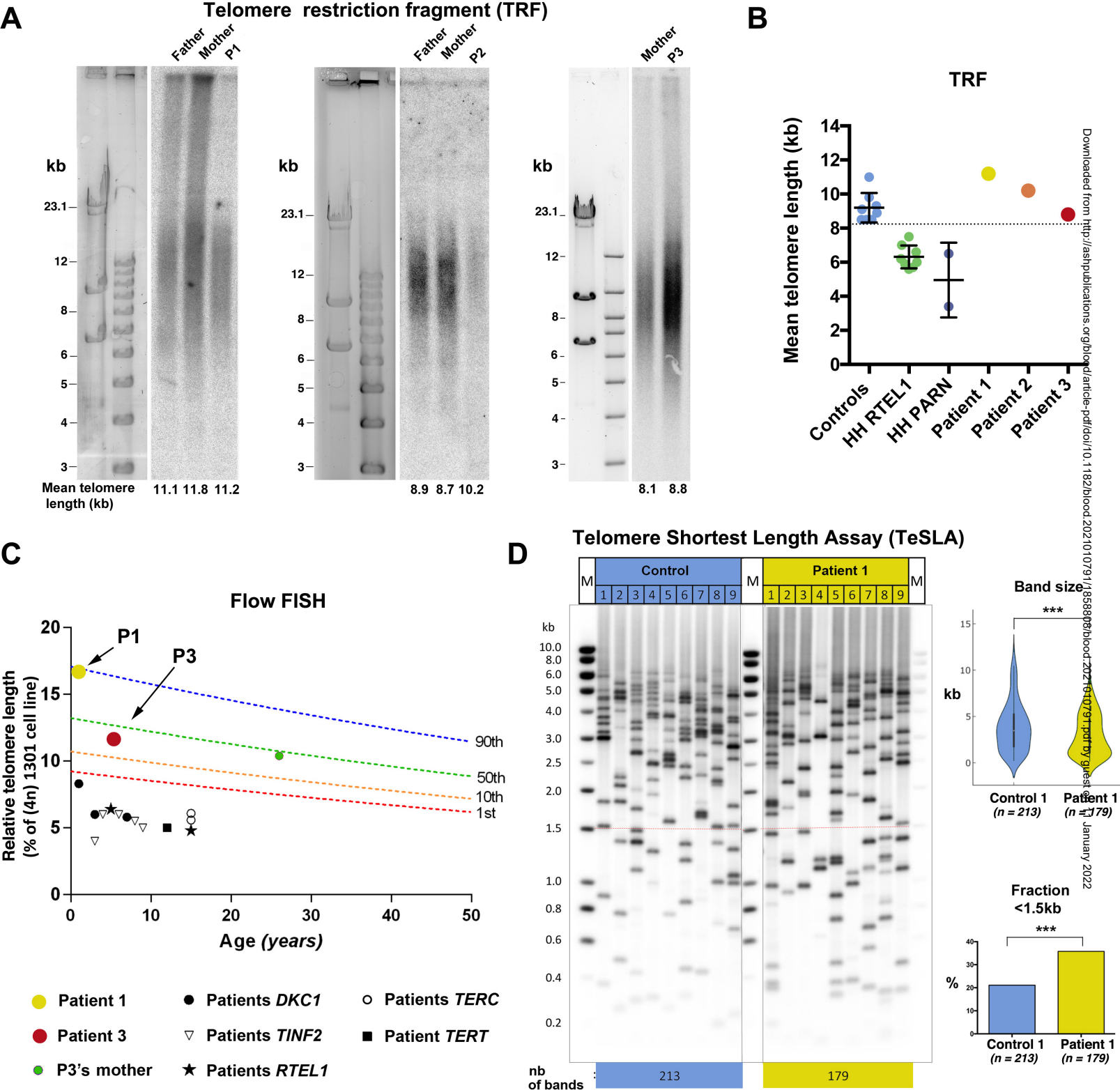
717

718

719 **Figure 4. Genome instability and DNA repair defect in patients' cells.** (A) Representative picture  
 720 of normal chromosomes, radial chromosomes and chromosome found in metaphase. (B-C)  
 721 Quantitative analysis of radial chromosomes (B) and chromosome breaks (C) in untreated and MMC-  
 722 treated cells. Cells from a Fanconi (FANC-G deficient) patient are used as a sensitive control.  
 723 Percentage of events per chromosomes is indicated (2 independent experiments); Counted  
 724 chromosomes: Ctrl -MMC:  $n = 583$ ; Ctl +MMC:  $n = 929$ ; P1 -MMC:  $n = 789$ ; P1 +MMC:  $n = 620$ ; P2 -  
 725 MMC:  $n = 710$ ; P2 +MMC:  $n = 674$ ; Fanconi -MMC:  $n = 811$ ; Fanconi +MMC:  $n = 965$ ). (D) MMC  
 726 sensitivity of SV40-transformed fibroblasts from P1 and P2, a Fanconi patient, and control. Mean and  
 727 standard deviation of triplicates are represented. Result representative of 4 independent experiments.  
 728 A two-tailed standard t-test was used. (E) Aphidicolin sensitivity of SV40-transformed fibroblasts from  
 729 P1 and P2, control, and control with ATR inhibitor (ATRi, 10 $\mu$ M). Mean and standard deviation of  
 730 triplicates are represented. Result representative of 3 independent experiments. A two-tailed standard  
 731 t-test was used. (F) Phleomycin sensitivity of SV40-transformed fibroblasts from P1 and P2, a  
 732 Cernunnos-deficient patient<sup>60</sup>, and a healthy control. Mean and standard deviation of triplicates are  
 733 represented. Result representative of 5 independent experiments. A two-tailed standard t-test was  
 734 used. (G) Schematic representation of the correction of one Apollo variant in P2's cells via  
 735 CRISPR/Cas9 generating a heterozygous Apollo-mutated P2 cell line (noted P2<sup>L142S/WT</sup>). (H)  
 736 Phleomycin sensitivity of hTERT SV40-fibroblasts from P2, P2<sup>L142S/WT</sup> and a healthy control. Mean and  
 737 standard deviation of triplicates are represented. Result representative of 3 independent experiments.  
 738 A two-tailed standard t-test was used.

739  
 740 **Figure 5. Telomere defects in HT1080 Apollo KO cell lines.** (A) Quantitative analysis of TIFs in the  
 741 two HT1080 Apollo KO clones and WT cells. (WT:  $n = 88$ , KO #1:  $n = 55$ ; KO #2:  $n = 66$ ). (B)  
 742 Quantitative analysis of telomeric aberrations detected by FISH. Percentage of events per  
 743 chromosomes (Counted chromosomes: WT:  $n = 715$ ; KO #1:  $n = 887$ ; KO #2:  $n = 528$ ). Averages and  
 744 chi-square tests were applied to compare Ctl with either P1 or P2. (C) (Up) Detection of the shortest  
 745 telomeres by TeSLA performed in WT HT1080 cell line and in the two Apollo KO HT1080 cell lines #1  
 746 and #2. (Down) Graphic representation of TeSLA data with statistical analyses. A two-tailed student t-  
 747 test was used for statistical analyses of band size and a  $\chi^2$  test was used for analysis of fraction <1kb.  
 748 (D) Measurement of G-overhang signal by native versus denatured in-gel hybridization method with C-  
 749 rich telomeric probe in WT and Apollo KO #1 HT1080 cell lines. The value of the 3' overhang was  
 750 normalized to the control. Values after correction for the effect of the telomere length are also  
 751 indicated (noted MTL\**Nat/den*). (E) Telomere length determined by telomere restriction fragment  
 752 (TRF) assay with DNA from the WT and the Apollo KO HT1080 cell lines #1 and #2.

**Figure 1**



Downloaded from <http://ashpublications.org/blood/article-pdf/doi/10.1182/blood.2021010791.1858808/blood-2021-010791.pdf> by guest on January 20, 2022



**Figure 2**

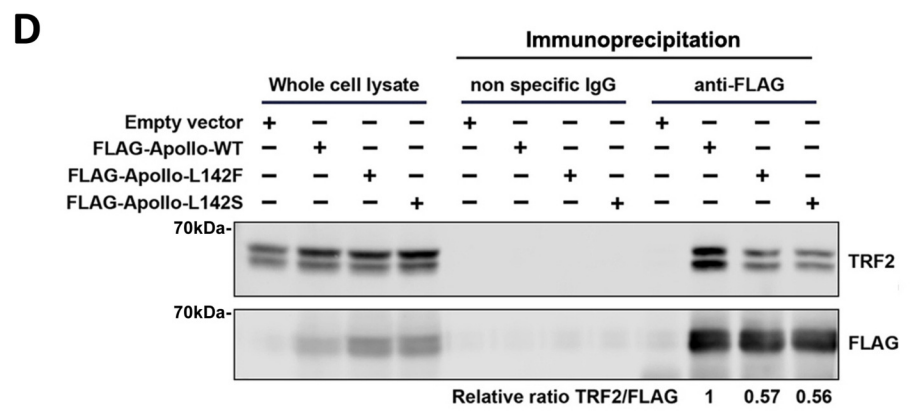
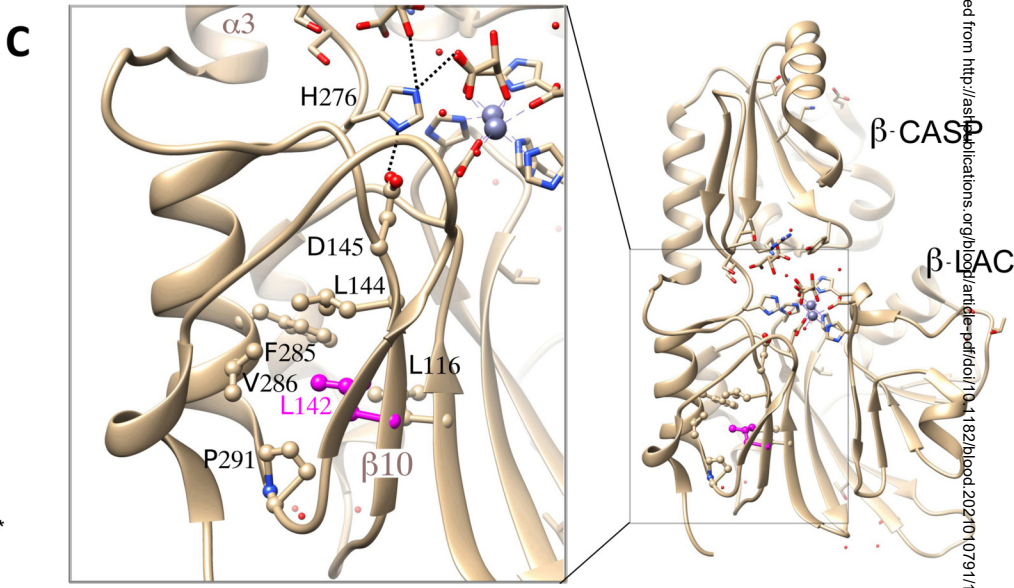
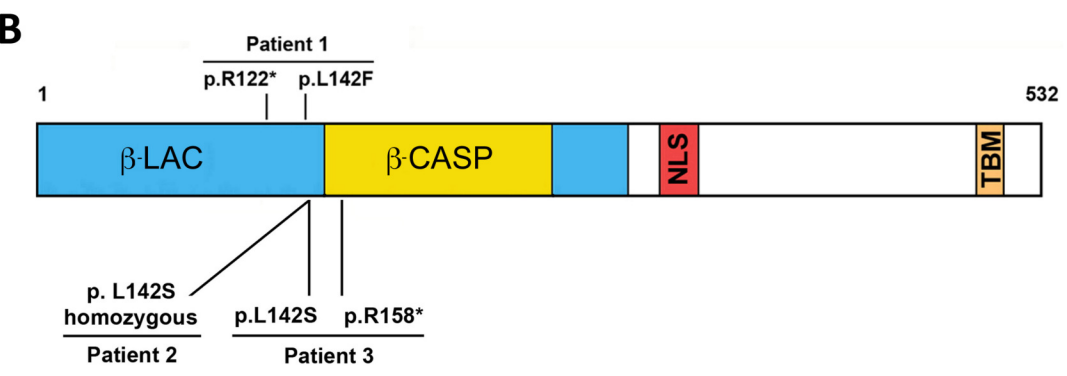
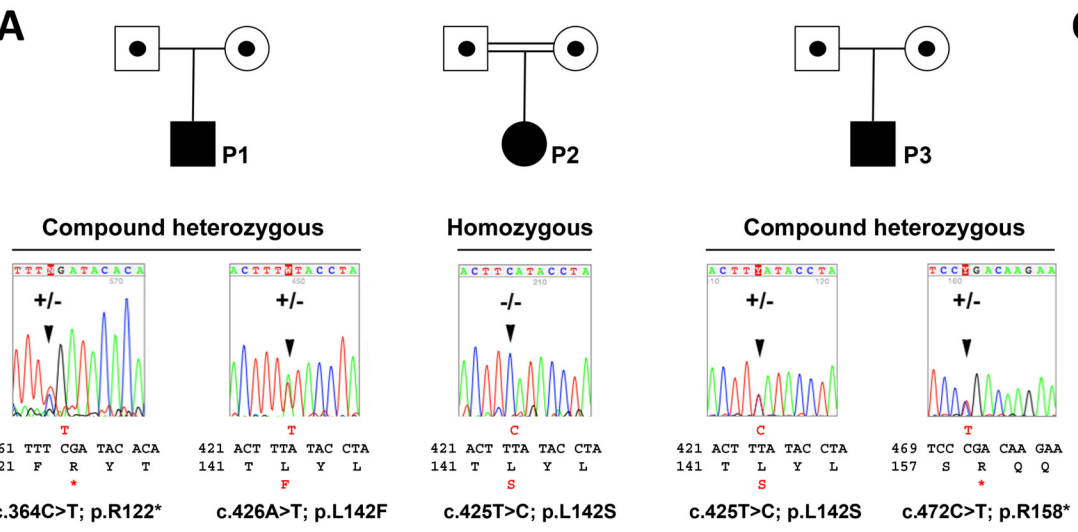


# Figure 3

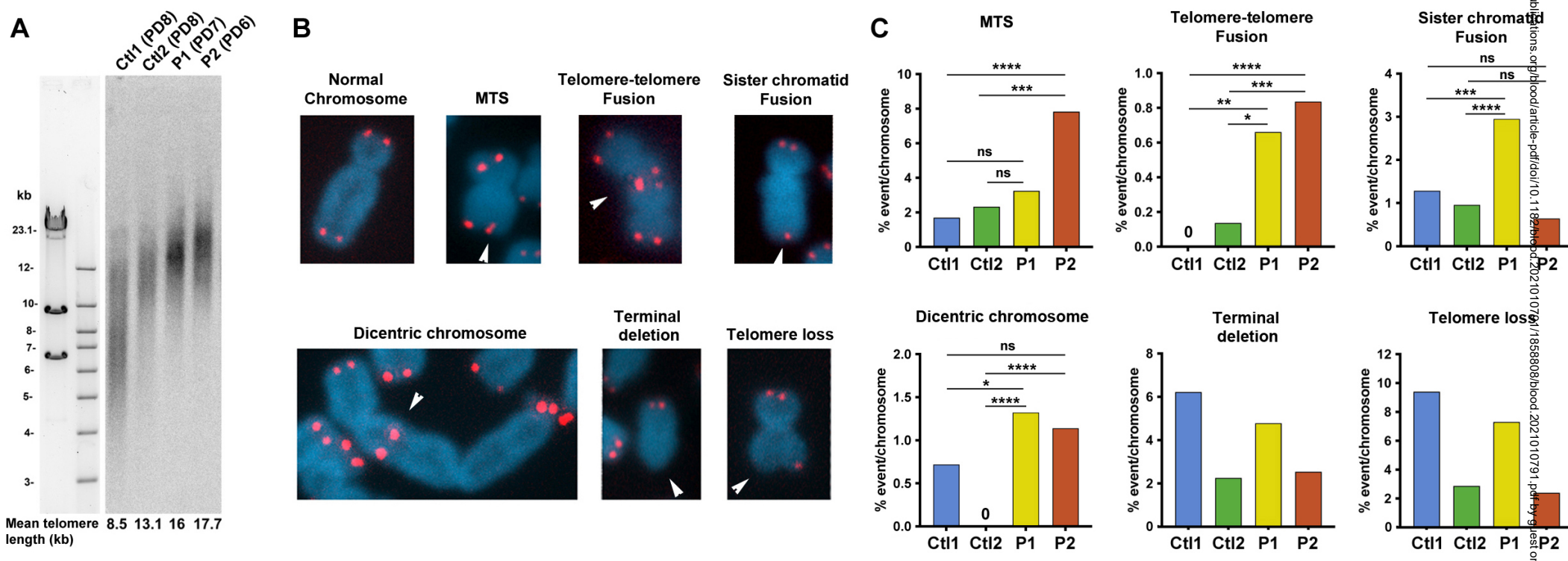
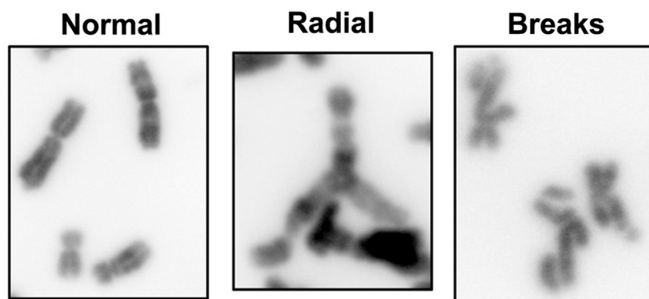
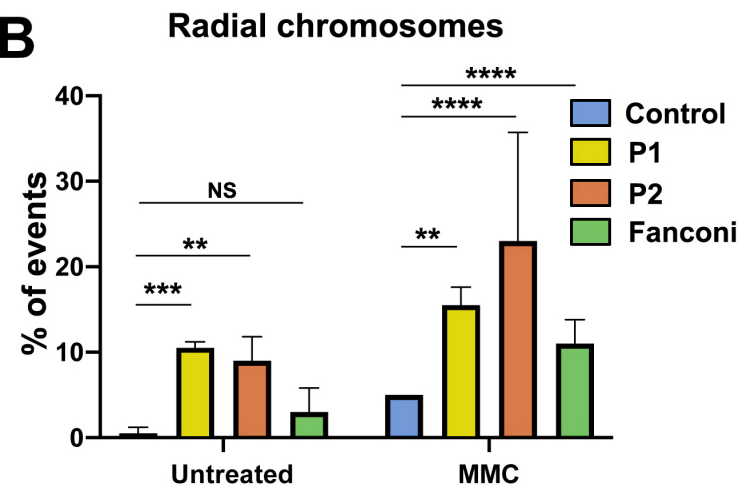


# Figure 4

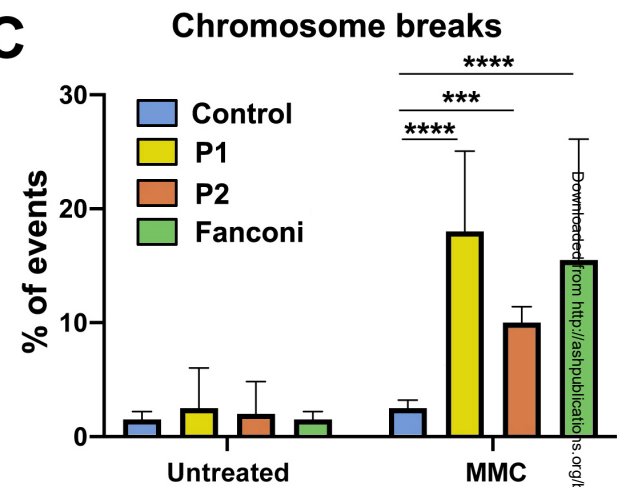
## A



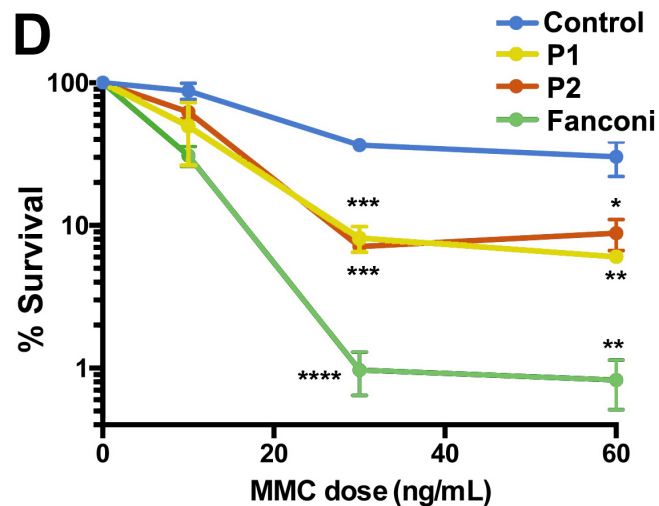
## B



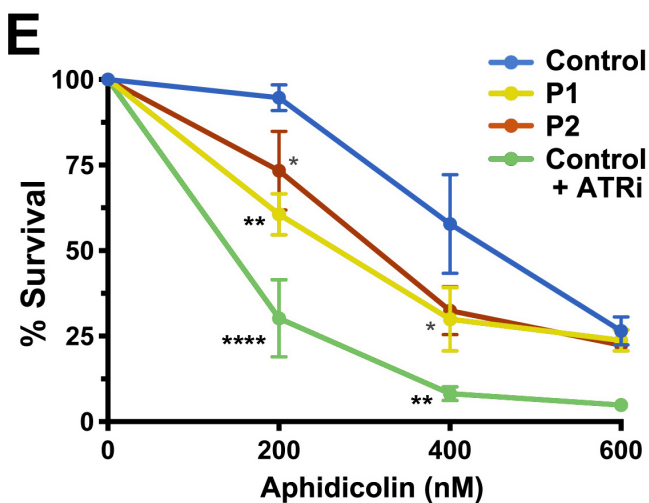
## C



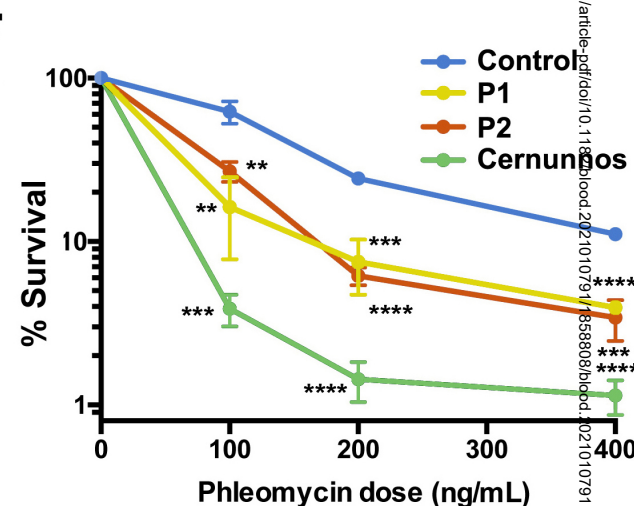
## D



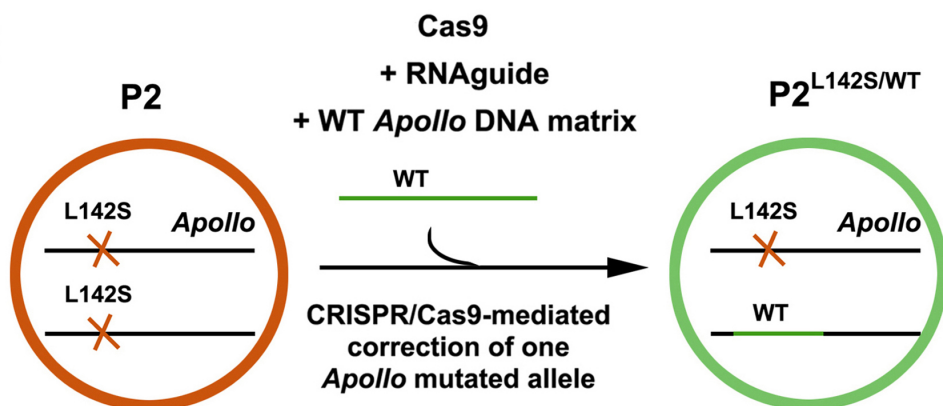
## E



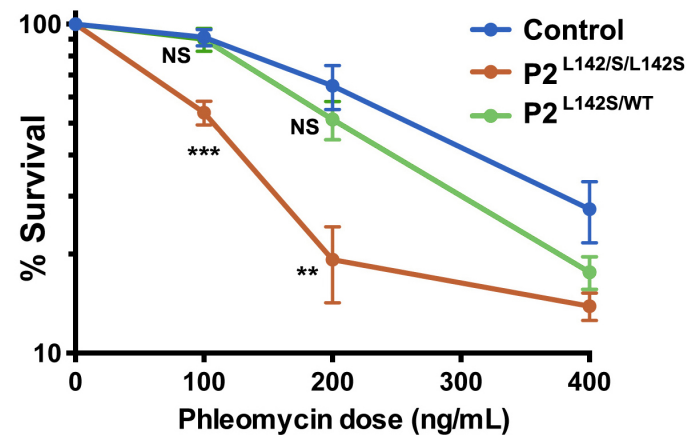
## F



## G

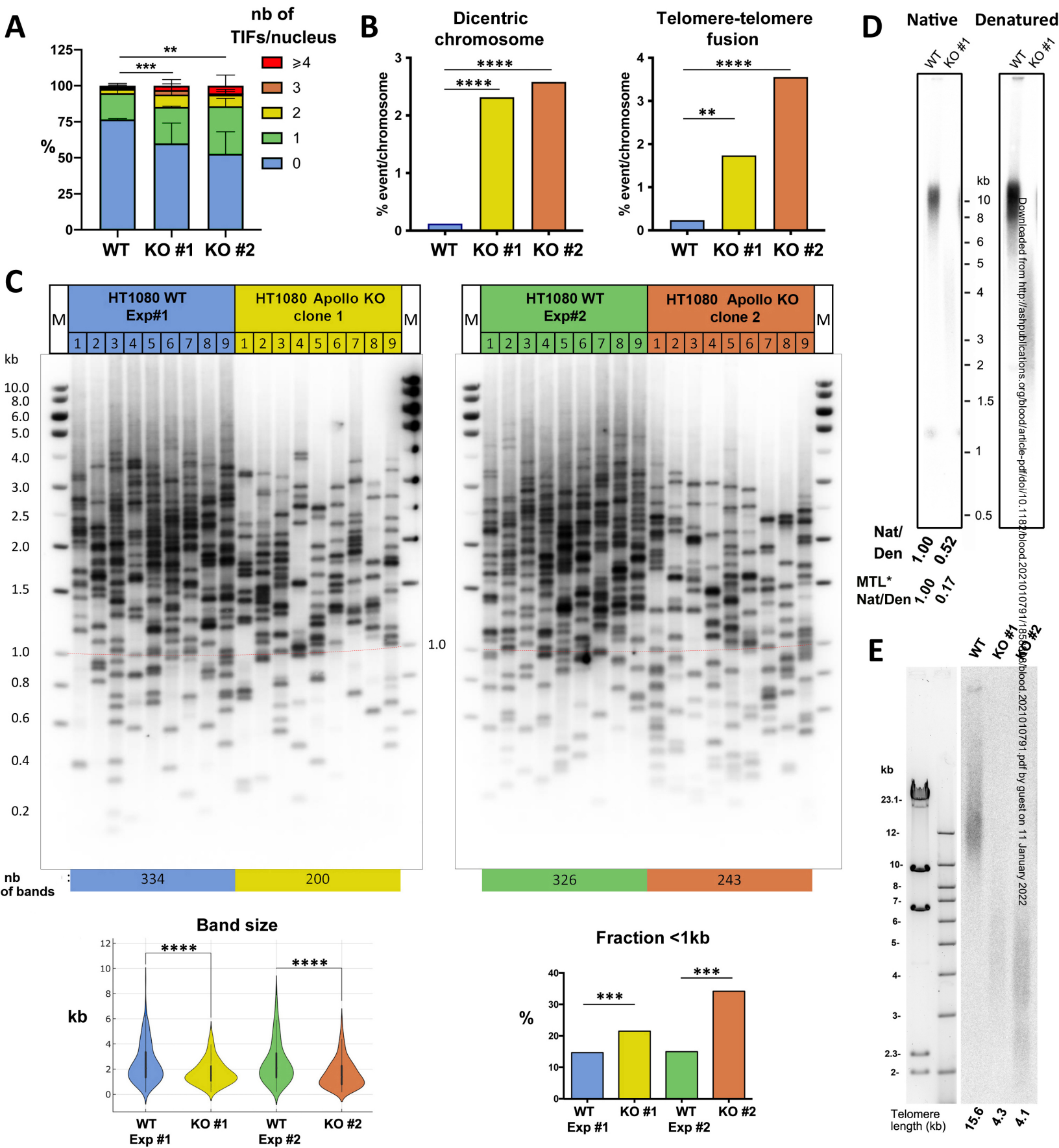


## H



Downloaded from <http://aspubs.aaapublications.org/food/article-pdf/doi/10.1111/food.2021010791> by guest on 11 January 2022

# Figure 5



Downloaded from <http://arxiv.org/abs/2021010791> by guest on 11 January 2022